Improving the sensitivity of WGM pressure sensors with Oxyfluoride glass microspheres

K. Soler-Carracedo[a], P. Estévez-Alonso[a], IR. Martin[a,b], S. Rios[a]

[a] Departamento de Física, Universidad de La Laguna. Apdo. 456. E-38200 San Cristóbal de La Laguna, Santa Cruz de Tenerife, Spain.

[b] Instituto Universitario de Materiales y Nanotecnología (IMN), Universidad de La Laguna. Apdo. 456. E-38200 San Cristóbal de La Laguna, Santa Cruz de Tenerife, Spain.

Abstract

Oxyfluoride glass microspheres doped Nd^{3+} were synthesized and calibrated to function as optical pressure sensors. When the microspheres were placed in a vacuum chamber and excited at 532 nm, Nd^{3+} typical emission spectrum was recorded. Due to the specific geometry of the microspheres, that allow them to act as an optical resonator, it was also possible to record Whispering Gallery Modes (WGM) superimposed to the Nd^{3+} typical emission spectrum. Furthermore, when decreasing pressure, changes in the Fluorescence Intensity Ratio (FIR) of the $^2H_{9/2}$,$^4F_{5/2}\rightarrow{}^4I_{9/2}$ (820 nm) and $^4F_{3/2}\rightarrow{}^4I_{9/2}$ (890 nm) Nd^{3+} transitions as well as a red-shift of the WGM was observed. Both changes were calibrated as a function of pressure. Relative sensitivity and limit of detection were estimated for both techniques as a way of comparing their performance, also taking into account the previous results found in the literature. Due to the high thermal expansion and thermo-optical coefficient of oxyfluoride glasses and the high energy gap of Nd^{3+} thermally coupled levels, the sensor presented groundbreaking levels of relative sensitivity and limit of detection.

Keywords: ultralow pressure; oxyfluoride glass; light-to-heat conversion; lanthanide ions; microsphere resonators

I. Introduction

The new era of technology keeps pushing the limits of sensing towards more precise, accurate and efficient sensors. Whether it is for science applications, industry or daily life uses; the needs to be met continue to grow with each passing year, and vacuum technology is becoming a key part for many of the previous mentioned applications. Current vacuum gauges are based on mechanical deformation [1,2], thermal conductivity [3–6], thermocouple or thermistor gauges; ionization [7,8] and spinning rotations [9]. With these gauges, uncertainties around 1 to 20% can be achieved. A new approach that has improved the aforementioned uncertainty values is the use of optical vacuum sensors. Up to date, the only researches following this approach were based on heterodyne [10,11] and optical fiber interferometry [12,13], resonance effects [14–16] or magneto-optical trapping [17] . In this paper, we continue the work of our previous publications [18,19], where we showed for the first time the possibility of converting a luminescence thermometer into an optical vacuum sensor, and later improved this sensor by using optical micro-resonators for a WGM emission [20] based sensor.

Oxyfluoride glasses are related to a type of materials, discovered in the 60s and labelled under the name of glass ceramics and/or vitroceramics [21]. Three decades later, these new type of glasses were doped with Er and Yb ions [22]. The novel material presented high upconversion efficiencies from the infrared to the green or the red, as well as high mechanical and chemical stability and high laser damage threshold [23–25]. Almost another three decades has passed since this discovery of oxyfluoride glasses, and the applications for this novel material are countless, from white and tunable LED light generation [26–28] to optical temperature sensors [29,30], including industrial applications [31,32], medical sensors, 3D displays, etc [33,34].

The sensitivity of WGM based sensors is related to changes in the size and refractive index of the optical micro-resonator [35]. Following this, the higher values of the thermal-expansion and thermo-optic coefficients of this material, among the other great optical properties aforementioned, make oxyfluoride glass a promising candidate for WGM optical pressure sensor.

II. Theoretical background

A. Technique

The FIR technique is one of the most common techniques used in optical sensors. This technique relies on a pair of energy levels with small energy separation, thermal energy bellow 2000 cm^{-1}, that can be found in various lanthanide (Ln^{3+}) doped materials. The small energy gap allows thermalization processes to occur and thus, the temperature can be estimated by the analysis of the band intensity ratio, associated with the excited thermally coupled levels of the selected Ln^{3+} ion.

For Nd^{3+} ions, the relative population between the levels can be described as a three level system that follows a Boltzmann type distribution [36]:

$$FIR(T) = \frac{I_{31}}{I_{21}} = \frac{\omega_{31}^{R} g_3 h v_3}{\omega_{21}^{R} g_2 h v_2} \exp\left(\frac{-E_{32}}{K_B T}\right) = C exp\left(\frac{-E_{32}}{K_B T}\right) \quad (1)$$

where I_{31} and I_{21} are the emission intensities of the transitions from level 3 to 1 and level 2 to 1, respectively; K_B is the Boltzmann constant, E_{32} is the energy gap between the two thermalized excited levels 2 and 3, g_3 and g_2 are the degeneracies $(2J+1)$ of these levels, v_3 and v_2 are the frequencies of the transitions from level 3 and 2 to ground state respectively and ω_{31}^{R} and ω_{21}^{R} are the spontaneous emission rates from the respective levels to the ground state and C is the pre-exponential factor. As it can be seen from Eq. (1), the FIR technique is independent of the incident pump-power source, as it affects only the intensity of both emissions bands, but not their intensity ratio, that is only dependent on the temperature.

Finally, due to the unique geometry of the microspheres, it is possible for the emitted light to get trapped inside the resonator in the form of WGM [37]. The spectral position of these WGM can be approximated to equation [35]:

$$\lambda_m = \frac{2\pi}{m} \cdot n_{eff} R \tag{2}$$

where m is the mode number, λ_m are the resonant wavelengths, n_{eff} is the effective refractive and R the radius of the microsphere. From Eq. (2), it follows that the displacement in the WGM spectral positions will be given by:

$$\frac{d\lambda_m}{\lambda_m} = \frac{dn_{eff}}{n_{eff}} + \frac{dR}{R} \tag{3}$$

this is, the variation in the WGM spectral position variations will be related to changes in both the effective refractive index and the radius of the microsphere. These variations can occur by means of temperature changes as well as changes in the hydrostatic pressure surrounding the microsphere [38]. In the case of temperature changes, the previous variations are described by the thermal expansion and thermo-optic coefficients [20]:

$$\frac{d\lambda_m}{dT} = \lambda_m \left(\frac{1}{R}\frac{dR}{dT} + \frac{1}{n_{eff}}\frac{dn_{eff}}{dT} \right) = \lambda_m(\alpha + \beta) \tag{4}$$

where α and β are the thermal expansion and thermo-optic coefficients, respectively. In the case of oxyfluoride glass, these coefficients are both positives and present a linear behavior with temperature in this range of temperatures [39]. Therefore, a red-shift is expected when the microsphere is heated.

For the variations related to the hydrostatic pressure, Ioppolo *et al.* [38] evaluated the stress and strain for a hollow polymer microsphere, obtaining an expression for the WGM shifts vs pressure, which can be extrapolated for a solid microsphere by considering a null internal diameter. For a microsphere subjected to an external pressure *P*, the effects of the applied mechanical stress on the radial component can be obtained by solving the elasticity equation in spherical coordinates, while the effects in the refractive index of the sphere is given by the Neumann-Maxwell equation [40]. Introducing both results in Eq. (3), the following expression is obtained:

$$\frac{d\lambda_m}{\lambda_m} = \frac{dR}{R} + \frac{dn_{eff}}{n_{eff}} = -P \left(\frac{1}{2G}\frac{1-2\nu}{1+\nu} + \frac{(C_1 + 2C_2)}{n_r} \right) = -P \left(\frac{1-2\nu}{E} + \frac{3C}{n_r} \right) \tag{5}$$

where G is the shear modulus, ν is the Poisson ratio of the material of the sphere, C are the elasto-optical constants ($C_1 = C_2 = C$ if the microsphere is considered an isotropic solid), n_r is the refractive index for the unstressed material in the radial direction and E is the Young modulus. From Eq. (5), it follows that for decreasing pressure, a red-shift is expected for the WGM spectral positions. However, given the high Young Modulus of most oxyfluoride glasses reported to date [41–43], whose values approximately range from 7.5×10^7 to 7.5×10^8 Torr, compared to the range used in this work, from 3.15 to 4.1×10^{-2} Torr, it can be assumed that the microspheres did not suffer any significant volume strain due to pressure, capable of affecting the measurements. As far as the change in the refractive index, the photoelasticity theory [44,45] relates the changes in the refractive index with density changes as well as, in a minor contribution, changes in the polarizability. Consequently, it is also safe to assume that no volume strain nor density change

that could lead to refractive index changes, would occur in the microsphere under this pressure range. The WGM spectral displacement observed as a function of pressure, must then be related to the temperature change of the microsphere as pressure decreases.

B. Sensitivity

To characterize the sensing capability of a material, it is to use the absolute sensitivity (S) has been used. It is described by the evolution rate of the sensing parameter as a response to the desired physical property, and is given by the formula:

$$S = \left|\frac{dM_p}{dT}\right| \tag{6}$$

where M_p is the aforementioned parameter.

However, this feature cannot be considered as a standard for comparison, due to its dependency on the nature of the sensing parameter and the experimental setup, among others. Thus, in order to compare different sensors, *Collins et al.* [46] defined another figure of merit denoted as the relative sensitivity (S_r) and given by:

$$S_r = \frac{1}{M_p}\left|\frac{dM_p}{d\mathrm{T}}\right| \tag{7}$$

which allows comparison of optical sensors, even if they are based on different physical parameters. The relative sensitivity is usually represented in % K^{-1} instead of just K^{-1}.

Another important parameter used to characterize the sensor is the limit of detection ($\delta M_{p_{min}}$), also known as uncertainty. This parameter is related to the minimum parameter change that the sensor is capable to recorded and it is given as:

$$\delta M_{p_{min}} = \frac{1}{S_r}\frac{\delta M_p}{M_p} \tag{8}$$

where $\delta M_p/M_p$ is the resolution limit or relative uncertainty of the thermometric parameter, this is, the smallest variation that can be experimentally detected.

In the case of WGM based sensors, it was previously mentioned how the dependence of the WGM spectral positions with temperature is related to the thermo-optic and thermal expansion coefficients of the material through Eq. (4). Furthermore, substituting this equation on the relative sensitivity, being M_p the spectral position of the WGM, leads to:

$$S_r = \frac{1}{\lambda_{WGM}}\left|\frac{d\lambda_{WGM}}{d\mathrm{T}}\right| = (\alpha + \beta) \tag{9}$$

This is, the relative sensitivity relies solely in the thermo-optic and thermal expansion coefficients of the material, neglecting other important aspect related to the WGM phenomenon such as morphology of the microsphere and the concentration of the RE ions. It must be taken into account however, that this conclusion is obtained by means of the geometrical optical-ray

approximation presented in Eq. (2) and that the optimization of the concentration of Nd^{3+} ions could improve the emission of the intensity and its reliability.

If we now introduce Eq. (4) into Eq. (8) we obtain, for the temperature uncertainty:

$$\delta T_{min} = \frac{1}{S_r} \frac{\delta \lambda_{WGM}}{\lambda_{WGM}} = \frac{\delta \lambda_{WGM}}{\lambda_{WGM}(\alpha + \beta)} \quad (10)$$

This is, the relative sensitivity, for WGM temperature based sensors, is exclusively related to the thermo-optics and thermal expansion coefficients of the material of the resonator. Whereas, for the limit of detection or temperature uncertainty, it is also dependent on the experimental setup [47]. Therefore, one way of improving the resolution limit could be the use of better acquisition systems, and also by configuring the measurements with longer integration time and averaging consecutive measurements to decrease experimental noise. However, such procedure increases the temporal response of the sensor, and delays determination of the measured function, which may be undesired in some applications. Improving the sensitivity of the sensor on the other hand, relies solely in finding materials with higher thermo-optics and thermal expansion coefficients.

Following the previous line of thought, a oxyfluoride glass microsphere doped with Nd^{3+} was synthesized and irradiated at constant power (3 mW) and the emission was recorded as a function of vacuum. Emission changes when surrounding pressure decreases are related to temperature increment in the microsphere. Consequently, it is possible to characterize the Nd^{3+} doped microspheres as an optical vacuum sensor. Considering Eq. (9), oxyfluoride glass structure was selected due to its high thermal expansion and thermo-optic coefficients, to surpass the sensitivity of its predecessors, based on soda-lime glass microspheres. For oxyfluoride glass $\beta \approx 21\text{x}10^{-6}\ ^{o}C^{-1}$ [35], one order of magnitude higher than typical values for soda lime glass with $\beta \approx 2.06\text{x}10^{-6}\ ^{o}C^{-1}$ [48]. Whereas for thermal expansion coefficients, the values are closer for both materials, with $\alpha \approx 10.85\text{x}10^{-6}\ ^{o}C^{-1}$ [49] for oxyfluoride glasses and $\alpha \approx 9.25\text{x}10^{-6}\ ^{o}C^{-1}$ [50] for soda-lime glass.

III. Experimental procedure

A. Sample preparation

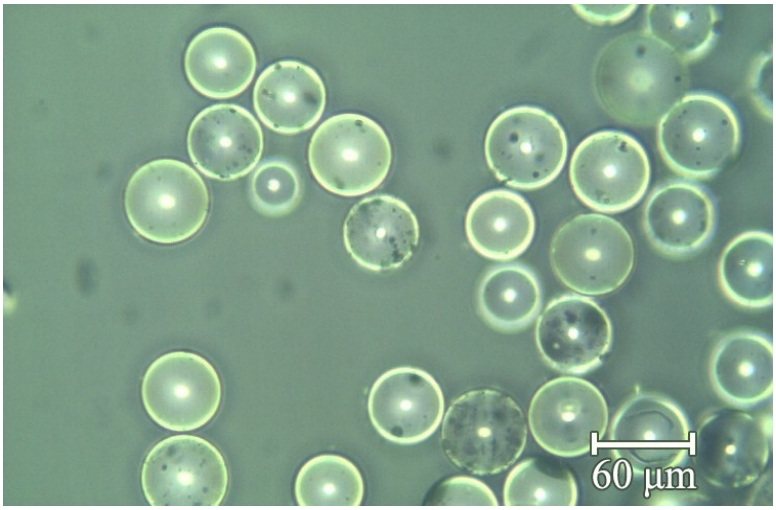

Fig. 1. Optical image of the resulting microspheres.

The oxyfluoride samples doped with Nd3+ used in this study have the following chemical composition (in mol%): $30SiO_2$, $15Al_2O_3$, $29CdF_2$, $22PbF_2$, $3YF_3$ and $1NdF_3$. To obtain the samples, the mixed composition was melted in an electric furnace at 1050 ºC for 2 h and the resulting melt was quickly casted into a slab by pressing between two stainless steel plates at RT [35]. To obtain microspheres, the resulting bulk sample was crushed to a fine powder in an agate mortar. The resulting powder was then dropped onto a horizontal butane flame, allowing the flame to produce liquid droplets from the powder. Due to the high surface tension, the droplets turned into spheres during the cooling process [19]. Highly transparent microspheres with diameters from 35 to 65 µm were obtained from the process (Fig. 1).

B. Optical characterization

The absorption spectrum was carried out with a double beam spectrophotometer, model Cary Series UV-vis-NIR Spectrophotometer from Agilent Technologies. Spectral emission was obtained by exciting the material with a continuous-wave 532 nm diode pumped solid state laser. For excitation and detection, a modified confocal microscope was used, collecting the light emitted by the sample with an objective and then focused it on the entrance slit of a grating spectrometer (Andor SR-500i-B2), coupled to a CCD (Newton 970EMCCD) detector. An adjustable mirror, combined with the entrance slit (~60 µm) acting as an image plane pinhole, allowed to partially detect the emission from localized parts of the microsphere [51].

To calibrate the optical response of the sample with temperature, luminescence measurements were carried out from 295 K (room temperature - RT) to 470 K in a tubular electric furnace (Gero RES-E 230/3), where the temperature of the sample was controlled via a type K thermocouple.

To calibrate the optical response of the sample with pressure, the microspheres were located inside a vacuum chamber. The vacuum was obtained by an oil pump (Edwards RV3), where the pressure gauge was connected to a digital controller (Edwards Active Gauge Controller Single Display).

All spectra were corrected from the spectral response of the equipment. To obtain the spectral resolution of the system, the width of a single mode laser line at 532 nm was measured at RT and ambient pressure, resulting in a spectral resolution of about 140 pm, in good agreement with the manufacturer specifications. For the resolution limit, 100 measurements of a laser profile under the same conditions were recorded. The spectra were fitted to a Gaussian curve and the uncertainty was calculated as the standard deviation of the laser peak position distribution. A standard deviation of 3 pm was obtained. Similar procedure was carried out to obtain the uncertainty of the FIR and WGM results at RT and 3.15 Torr. For the WGM results, 100 measurements from a single peak were made and the peak centroid was reported by means of the cubic spline interpolating method. Standard deviations of $7 \cdot 10^{-4}$ and 5.5 pm for the FIR intensity ratio and WGM spectral positions were obtained, respectively. A deviation given by the double of the uncertainty was used for the error bars, in the figures representing the FIR and WGM results.

III. Results and discussion

A. Optical response to temperature

Fig. 2 shows the absorption spectrum of oxyfluoride glass doped Nd^{3+} where the neodymium absorption bands can be seen, assigned to their respective transitions, from 350 to 800 nm.

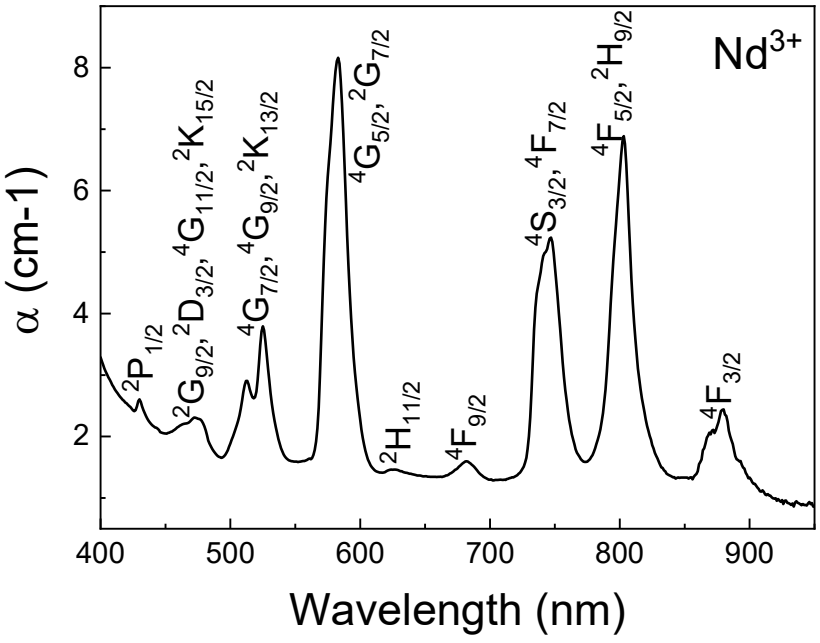

Fig. 2. Absorption spectrum of oxyfluoride glass doped with Nd3+, were the peaks correspond to transitions from the $^4I_{9/2}$ fundamental level.

The emission spectrum from a microsphere of oxyfluoride glass doped with Nd^{3+}, under 532 nm excitation, can be seen in Fig. 3 (black dashed line). Three broad emissions bands can be seen in the near infrared range of the spectrum, corresponding to the $^2H_{9/2}$,$^4F_{5/2} \rightarrow {}^4I_{9/2}$, $^4F_{3/2} \rightarrow {}^4I_{9/2}$ and $^4F_{3/2} \rightarrow {}^4I_{11/2}$ Nd^{3+} transitions at 820, 890 and 1064 nm, respectively. When the confocal setup was

used and the detection was set to an edge of the microsphere, to selectively detect the light trapped inside the microsphere in the form of WGM, the spectrum drastically changed. A series of narrow peaks (blue continuous line), corresponding to the WGM phenomenon, appeared superimposed to the previous emission spectrum.

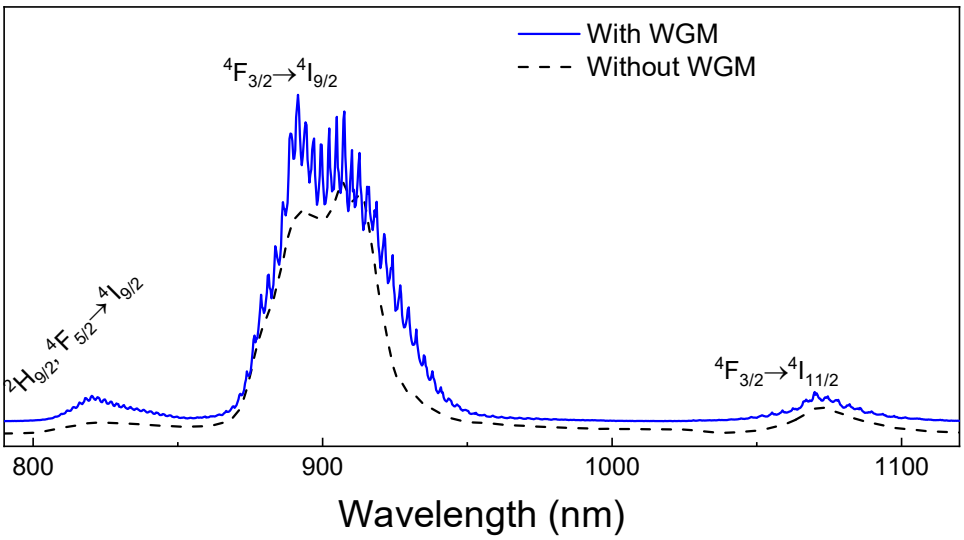

Fig. 3. Regular (black-dashed) and WGM (blue-continuous) emission of the TGC2:Nd^{3+} microsphere, under 532 nm excitation.

To obtain the thermal dependence of the emission, the sample was heated inside a tubular furnace and irradiated at 532 nm with low laser power (3 mW), in order to avoid laser heating processes. As the temperature of the furnace increased, the band Intensity Ratio (FIR) between the $^2H_{9/2}$,$^4F_{5/2}\rightarrow{}^4I_{9/2}$ (820 nm) and $^4F_{3/2}\rightarrow{}^4I_{9/2}$ (890 nm) Nd^{3+} transitions changed. Fig. 3a. shows the FIR results from the aforementioned bands from RT to 470 K. The results were fitted to Eq. (1), leading to an energy difference for the Nd^{3+} TCL of $E = 901\ cm^{-1}$, in good agreement with the previous literature [19,52,53] for different matrices.

To measure the WGM emission as a function of temperature, the microsphere was laser-heating by increasing the incident pump-power, and the local temperature was determined using the previous calibration. When heating the microsphere, another phenomenon was observed. The spectral positions of the WGM shifted towards the red when increasing the temperature, as it was expected following Eq. (4) for oxyfluoride glass, a material with positive thermo-optic and thermal expansion coefficients. In Fig. 4b, it can be seen the mean WGM shift as a function of temperature for four different resonant modes from the 890 nm Nd^{3+} emission band. The error bar used for the temperature axis were obtained from the standard error of a type-K thermocouple. For the FIR and WGM shift results, the double of the uncertainty value, obtained as it was explained in Optical Characterization section, was used as error bars.

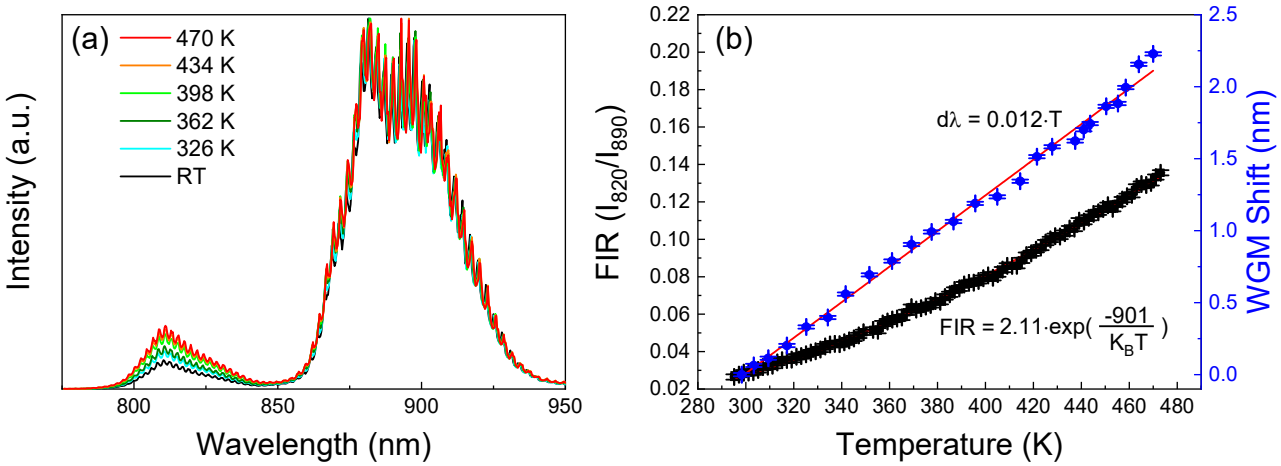

Fig. 4. a) Emission of the TGC2:Nd^{3+} sample as a function of temperature. **b)** FIR (black squares) and WGM shift (blue dots) as a function of temperature, fitted to Eq. (1) and Eq. (4), respectively (red lines).

B. Optical response to pressure

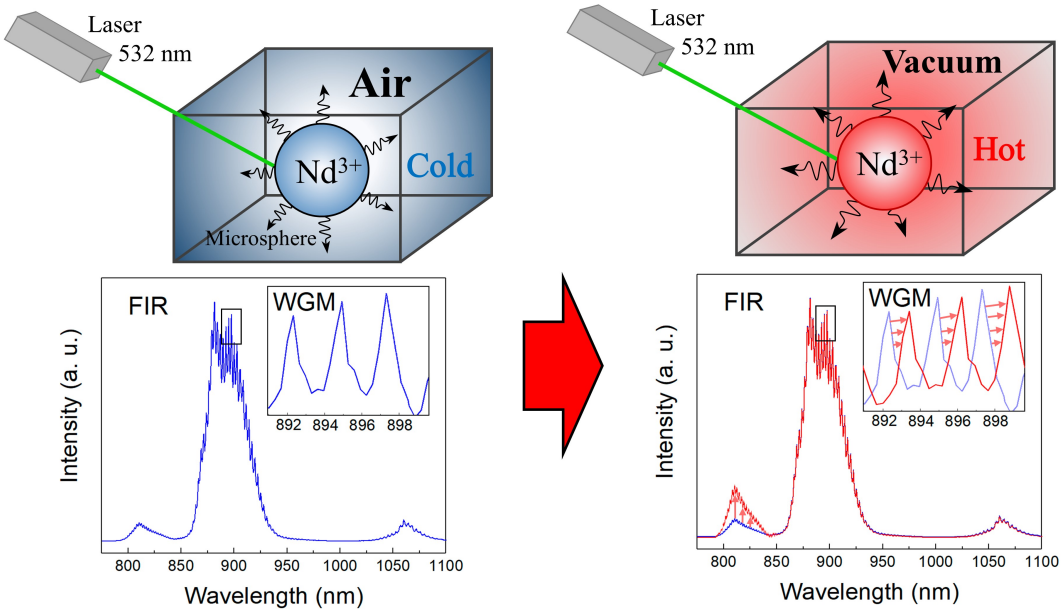

Fig. 5. Schematics representation of the pressure sensor based on the FIR technique and the WGM spectral shift for a Nd^{3+} microsphere.

To analyze the emission of the sample as a function of pressure, the microsphere was located inside a vacuum chamber and pumped with a 532 nm laser (see Fig. 5). When decreasing the pressure of the chamber, the FIR between the Nd^{3+} transitions change similarly to when the sample was placed inside the furnace to increase the temperature. The spectra were recorded from 3.15 to 4.1×10^{-2} Torr, and the FIR results can be seen in Fig. 6a. Technical limitations of the vacuum system did not allow to calibrate the sensor for pressures below 4.1×10^{-2} Torr. Furthermore, a red-shift was also observed in the spectral position of the WGM emission as pressure decreased (Fig. 5). This WGM spectral shift was recorded for several peaks, as a function of pressure, in the same range from 3.15 to 4.1×10^{-2} Torr. The mean shift for four

different resonant modes is represented in Fig. 6b. Following the manufacturer specifications, for the pressure error bars, 0.1, 0.01 and 0.001 Torr were used for the 10^{0}, 10^{-1} and 10^{-2} Torr ranges, respectively. For the WGM shift, the error bars were set as the double of the uncertainty value, like it was described in the Optical Characterization section. For both cases, the associated local temperature change, obtained through the FIR calibration, is presented in the upper axis of Fig. 6.

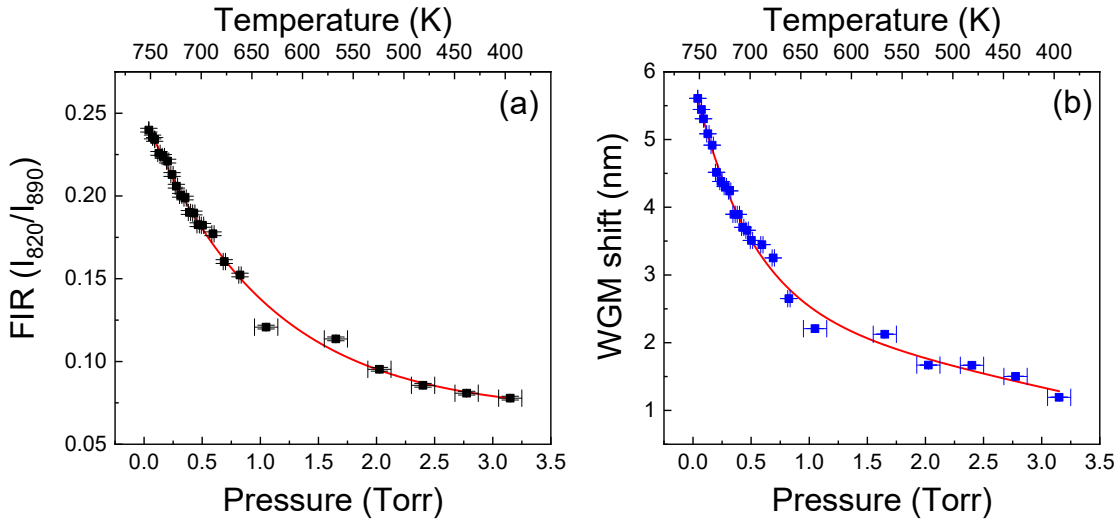

Fig. 6. a) FIR and **b)** WGM spectral shift for the Nd^{3+} microspheres as a function of vacuum.

From 3.15 to $4.1x10^{-2}$ Torr, the FIR had a variation of approximately 0.16 whereas the WGM resonant modes had a shift of approximately 4 nm. Furthermore, a non-linear behavior was observed when measuring in the previous range for both, the FIR and the WGM shift results. With a clear increase on the rate for both techniques at around 1 Torr. For the FIR technique, a similar phenomenon has already been observed by *Ben McMillen et al.* [12] when measured vacuum with a fiber Bragg grating at constant power, among others [19]. Giving that the experiment works with hydrostatic pressure, extracting air from the chamber with a vacuum pump (decrease of the number of particles) at fixed volume and temperature, the pressure decrease due to the fact that decreasing the number of particles increase the mean free path of particles inside the chamber and leading to lesser collisions with the chamber walls. When the air pressure of the chamber reaches 1 Torr, the mean free path of the air particles is similar or greater than the distance between the microsphere and the walls of the vacuum chamber [12], which could explain the different behaviors below and over 1 Torr observed in Fig. 6. This change in the behavior is more clear in the case of the WGM, as these modes should have a linear dependence with respect to both, temperature and pressure, following Eq. (4) and Eq. (5), respectively.

As it was stated in the Theoretical Background section, the WGM spectral displacement due to the effect of pressure is negligible in the range of the experiment. The observed red-shift must be then related to an increase of the temperature on the microsphere. For a microsphere under low-pump power laser excitation, the heat loss occurs through conduction by the surrounding gas and radiation [54]. As pressure decreases, the thermal exchange due to the conduction between the microsphere and the surrounding air molecules also decreases, which leads to the observed temperature increase on the microsphere.

From the fittings of Fig. 6, the relative sensitivity and limit of detection were obtained using Eq. (7) and Eq. (8), respectively. The results are shown in Fig. 7.

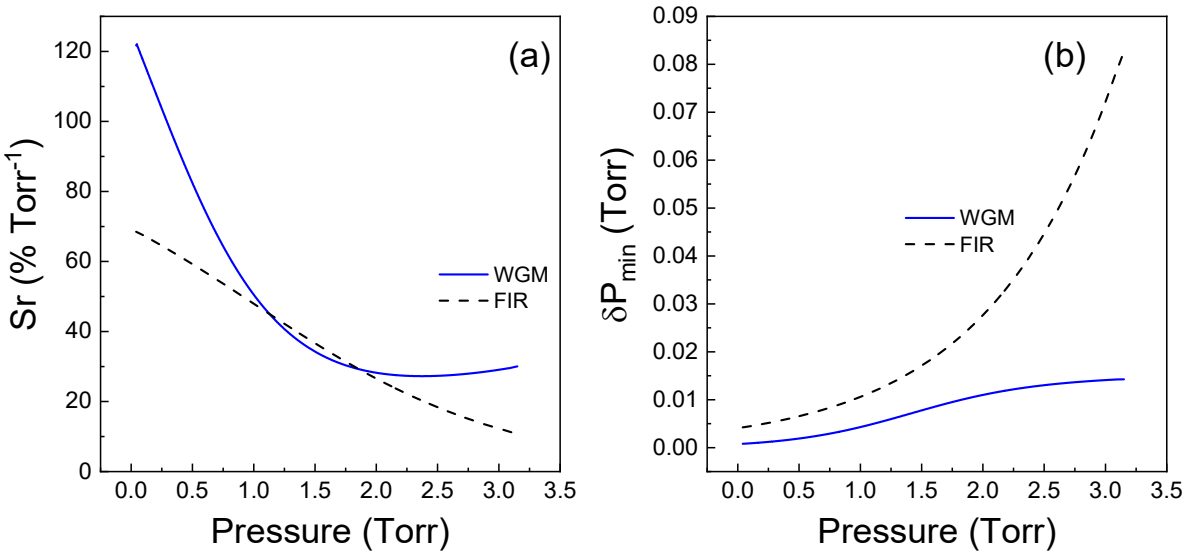

Fig. 7. a) Relative sensitivity and **b)** limit of detection for the FIR (black-dashed) and WGM spectral shift (blue-continuous) for the Nd^{3+} microspheres as a function of vacuum.

As it can be seen in Fig. 7, the use WGM spectral position for pressure calibration presents higher sensitivity and lower uncertainties in the whole range of pressure. The highest relative sensitivity for both techniques is achieved in the pressure range from 1 to $4.1x10^{-2}$ Torr, with maxima of 122% $Torr^{-1}$ for the WGM detection and 68% $Torr^{-1}$ for the FIR technique, both at $4.1x10^{-2}$ Torr. Whereas in the range from 3.15 to 1 Torr, both techniques have minima of 27% $Torr^{-1}$ for the WGM at 2.36 Torr and 11% $Torr^{-1}$ for the FIR at 3.15 Torr. When compare to its predecessor [19], this new sensor reported relative sensitivity values that are from one to three orders of magnitude higher for the whole pressure range. This result highlights the importance that the thermal expansion and thermo-optic coefficients of the material have in the sensitivity of the sensor, as it was previously discussed in the Theoretical Background section. Furthermore, the limit of detection also improved in the 3.15 to 1 Torr pressure range, while maintain similar values for lower pressures.

IV. Conclusions

Oxyfluoride glass microspheres doped with Nd^{3+} have been synthesized. When pumped under a low cost diode excitation laser at 532 nm, typical emission of the Nd^{3+} ions as well as WGM emission due to the unique geometry of the microsphere were recorded and calibrated as a function of temperature. By correlating the enhancement of the laser-induced heating of the lanthanide doped microsphere in a vacuum chamber, it was then possible to calibrate both the FIR technique and the WGM spectral positions for ultralow pressure sensing in the "near-infrared biological window" (650-950 nm). Relative sensitivity and limit of detection were calculated for the sensor. WGM presented better relative sensitivity values as well as lower uncertainties for the whole range of pressures. Furthermore, given the high thermal expansion and thermo-optic coefficients of oxyfluoride glass, the new developed sensor exhibited relative sensitivity values that surpassed its predecessor in various orders of magnitude.

Acknowledgments

The authors wish to thank financial support from Ministerio de Ciencia e Innovación of Spain (MICIIN) under the National Program of Sciences and Technological Materials (PID2019-106383GB-C44 and PID2019- 107335RA-I00) and Gobierno de Canarias (ProID2020010067) and EU-FEDER funds.

References

[1] J.J. Sullivan, Development of variable capacitance pressure transducers for vacuum applications, J. Vac. Sci. Technol. A Vacuum, Surfaces, Film. 3 (1985) 1721–1730. doi:10.1116/1.573008.

[2] K. Harada, K. Ikeda, H. Kuwayama, H. Murayama, Various applications of resonant pressure sensor chip based on 3-D micromachining, Sensors Actuators A Phys. 73 (1999) 261–266. doi:10.1016/S0924-4247(98)00245-3.

[3] R.E. Ellefson, A.P. Miiller, Recommended practice for calibrating vacuum gauges of the thermal conductivity type, J. Vac. Sci. Technol. A Vacuum, Surfaces, Film. 18 (2000) 2568. doi:10.1116/1.1286024.

[4] A. Berman, Total pressure measurements in vacuum technology, Academic Press, 2014.

[5] J.M. Lafferty, Foundations of vacuum science and technology, Wiley New York, 1998.

[6] F.T. Zhang, Z. Tang, J. Yu, R.C. Jin, A micro-Pirani vacuum gauge based on micro-hotplate technology, Sensors Actuators A Phys. 126 (2006) 300–305. doi:10.1016/j.sna.2005.10.016.

[7] C. Dong, G.R. Myneni, Carbon nanotube electron source based ionization vacuum gauge, Appl. Phys. Lett. 84 (2004) 5443–5445. doi:10.1063/1.1767956.

[8] W.C. Schuemann, Ionization Vacuum Gauge with Photocurrent Suppression, Rev. Sci. Instrum. 34 (1963) 700–702. doi:10.1063/1.1718549.

[9] J.K. Fremerey, The spinning rotor gauge, J. Vac. Sci. Technol. A Vacuum, Surfaces, Film. 3 (1985) 1715–1720. doi:10.1116/1.573007.

[10] M.-H. Chiu, J.-Y. Lee, D.-C. Su, K.-H. Lee, Vacuum measurement using total-internal-reflection heterodyne interferometry, Precis. Eng. 23 (1999) 260–263. doi:10.1016/S0141-6359(99)00019-7.

[11] K.-H. Chiang, M.-C. Hsieh, J.-Y. Lin, Phase-sensitive total-internal-reflection sensing system for measuring vacuum pressure, Opt. Laser Technol. 115 (2019) 508–513. doi:10.1016/j.optlastec.2019.02.060.

[12] B. McMillen, C. Jewart, M. Buric, K.P. Chen, Y. Lin, W. Xu, Fiber Bragg grating vacuum sensors, Appl. Phys. Lett. 87 (2005) 234101. doi:10.1063/1.2140082.

[13] K. Totsu, Y. Haga, M. Esashi, Vacuum sealed ultra miniature fiber-optic pressure sensor using white light interferometry, in: TRANSDUCERS '03. 12th Int. Conf. Solid-State Sensors, Actuators Microsystems. Dig. Tech. Pap. (Cat. No.03TH8664), IEEE, n.d.: pp. 931–934. doi:10.1109/SENSOR.2003.1215628.

[14] D. Uttamchandani, K.E.B. Thornton, J. Nixon, B. Culshaw, Optically excited resonant diaphragm pressure sensor, Electron. Lett. 23 (1987) 152. doi:10.1049/el:19870107.

[15] S. Inaba, K. Hane, Resonance frequency of a photothermal vibration for a polyethylene thin plate in medium vacuum region, J. Vac. Sci. Technol. A Vacuum, Surfaces, Film. 9 (1991) 3173–3174. doi:10.1116/1.577140.

[16] S. Inaba, K. Hane, Optical sensing for pressure in a medium vacuum region by using the drum effect, Appl. Opt. 31 (1992) 2969. doi:10.1364/AO.31.002969.

[17] T. Arpornthip, C.A. Sackett, K.J. Hughes, Vacuum-pressure measurement using a magneto-optical trap, Phys. Rev. A. 85 (2012) 033420. doi:10.1103/PhysRevA.85.033420.

[18] M. Runowski, P. Woźny, S. Lis, V. Lavín, I.R. Martín, Optical Vacuum Sensor Based on Lanthanide Upconversion—Luminescence Thermometry as a Tool for Ultralow Pressure Sensing, Adv. Mater. Technol. 5 (2020) 1901091. doi:10.1002/admt.201901091.

[19] K. Soler-Carracedo, I.R. Martin, M. Runowski, L.L. Martín, F. Lahoz, A.D. Lozano-Gorrín, F. Paz-Buclatin, Luminescent Nd 3+ -Based Microresonators Working as Optical Vacuum Sensors, Adv. Opt. Mater. 8 (2020) 2000678. doi:10.1002/adom.202000678.

[20] M.R. Foreman, J.D. Swaim, F. Vollmer, Whispering gallery mode sensors, Adv. Opt. Photonics. 7 (2015) 168. doi:10.1364/AOP.7.000168.

[21] S.D. Stookey, Method of making ceramics and product thereof, (1960).

[22] Y. Wang, J. Ohwaki, New transparent vitroceramics codoped with Er 3+ and Yb 3+ for efficient frequency upconversion, Appl. Phys. Lett. 63 (1993) 3268–3270. doi:10.1063/1.110170.

[23] Q.J. Chen, W.J. Zhang, X.Y. Huang, G.P. Dong, M.Y. Peng, Q.Y. Zhang, Efficient down- and up-conversion of Pr3+–Yb3+ co-doped transparent oxyfluoride glass ceramics, J. Alloys Compd. 513 (2012) 139–144. doi:10.1016/j.jallcom.2011.10.007.

[24] R. Lisiecki, W. Ryba-Romanowski, Silica-based oxyfluoride glass and glass-ceramic doped with Tm3+ and Yb3+ -VUV-VIS-NIR spectroscopy and optical thermometry, J. Alloys Compd. 814 (2020) 152304. doi:10.1016/j.jallcom.2019.152304.

[25] X. Chen, Z. Song, N. Sawanobori, M. Ohtsuka, X. Li, Y. Wang, X. Xu, C. He, H. Ma, Y. Chen, J. Zhu, The characteristic saturation phenomenon of upconversion luminescence in holmium–ytterbium-co-doped oxyfluoride glass Ho(0.1)Yb(5):FOG, Phys. B Condens. Matter. 403 (2008) 3847–3852. doi:10.1016/j.physb.2008.05.003.

[26] P. Babu, K.H. Jang, C.S. Rao, L. Shi, C.K. Jayasankar, V. Lavín, H.J. Seo, White light generation in Dy^3+-doped oxyfluoride glass and transparent glass-ceramics containing CaF_2 nanocrystals, Opt. Express. 19 (2011) 1836. doi:10.1364/OE.19.001836.

[27] Y. Ma, X. Peng, M. Fei, W. Zhang, L. Teng, F. Hu, R. Wei, H. Guo, Adjustable

white luminescence and high thermal stability in Eu2+/Eu3+/Tb3+/Al co-doped aluminosilicate oxyfluoride glass, J. Alloys Compd. 846 (2020) 156435. doi:10.1016/j.jallcom.2020.156435.

[28] R. Wang, D. Zhou, J. Qiu, Y. Yang, C. Wang, Color-tunable luminescence in Eu3+/Tb3+ co-doped oxyfluoride glass and transparent glass–ceramics, J. Alloys Compd. 629 (2015) 310–314. doi:10.1016/j.jallcom.2014.12.233.

[29] S. González-Pérez, I.R. Martín, F. Rivera-López, F. Lahoz, Temperature dependence of Nd3+→Yb3+ energy transfer processes in co-doped oxyfluoride glass ceramics, J. Non. Cryst. Solids. 353 (2007) 1951–1955. doi:10.1016/j.jnoncrysol.2007.01.059.

[30] W. Xu, X. Gao, L. Zheng, Z. Zhang, W. Cao, An optical temperature sensor based on the upconversion luminescence from Tm3+/Yb3+ codoped oxyfluoride glass ceramic, Sensors Actuators B Chem. 173 (2012) 250–253. doi:10.1016/j.snb.2012.07.009.

[31] A. Lipovskii, E. Kolobkova, V. Petrikov, I. Kang, A. Olkhovets, T. Krauss, M. Thomas, J. Silcox, F. Wise, Q. Shen, S. Kycia, Synthesis and characterization of PbSe quantum dots in phosphate glass, Appl. Phys. Lett. 71 (1997) 3406–3408. doi:10.1063/1.120349.

[32] G.H. Beall, L.R. Pinckney, Nanophase Glass-Ceramics, J. Am. Ceram. Soc. 82 (2004) 5–16. doi:10.1111/j.1151-2916.1999.tb01716.x.

[33] D. Ehrt, Photoluminescence in glasses and glass ceramics, IOP Conf. Ser. Mater. Sci. Eng. 2 (2009) 012001. doi:10.1088/1757-899X/2/1/012001.

[34] D. Ehrt, Photoactive glasses and glass ceramics, IOP Conf. Ser. Mater. Sci. Eng. 21 (2011) 012001. doi:10.1088/1757-899X/21/1/012001.

[35] K. Soler-Carracedo, A. Ruiz, I.R. Martín, F. Lahoz, Luminescence whispering gallery modes in Ho3+ doped microresonator glasses for temperature sensing, J. Alloys Compd. 777 (2019) 198–203. doi:10.1016/j.jallcom.2018.10.297.

[36] S.A. Wade, S.F. Collins, G.W. Baxter, Fluorescence intensity ratio technique for optical fiber point temperature sensing, J. Appl. Phys. 94 (2003) 4743. doi:10.1063/1.1606526.

[37] T. Reynolds, N. Riesen, A. Meldrum, X. Fan, J.M.M. Hall, T.M. Monro, A. François, Fluorescent and lasing whispering gallery mode microresonators for sensing applications, Laser Photon. Rev. 11 (2017) 1600265. doi:10.1002/lpor.201600265.

[38] T. Ioppolo, M.V. Ötügen, Pressure tuning of whispering gallery mode resonators, J. Opt. Soc. Am. B. 24 (2007) 2721. doi:10.1364/JOSAB.24.002721.

[39] F. Paz-Buclatin, S. Ríos, I.R. Martín, L.L. Martin, Fluorescence intensity ratio and whispering gallery mode techniques in optical temperature sensors: comparative study, Opt. Mater. Express. 9 (2019) 4126. doi:10.1364/OME.9.004126.

[40] P.S. Theocaris, E.E. Gdoutos, Matrix theory of photoelasticity, Springer, 2013.

[41] S.D. Patil, V.M. Jali, R. V. Anavekar, Elastic properties of Na2O-ZnO-ZnF2-

B2O3 oxyfluoride glasses, Bull. Mater. Sci. 32 (2009) 597–601. doi:10.1007/s12034-009-0091-z.

[42] I.Z. Hager, Elastic moduli of boron oxyfluoride glasses: experimental determinations and application of Makishima and Mackenzie's theory, J. Mater. Sci. 37 (2002) 1309–1313.

[43] I.Z. Hager, H.A. Othman, D.T. Valiev, Compositional dependence of thermal, optical and mechanical properties of oxyfluoride glass, J. Phys. Conf. Ser. 830 (2017) 012125. doi:10.1088/1742-6596/830/1/012125.

[44] H. Mueller, Theory of Photoelasticity in Amorphous Solids, Physics (College. Park. Md). 6 (1935) 179–184. doi:10.1063/1.1745316.

[45] H. Mueller, Theory of the Photoelastic Effect of Cubic Crystals, Phys. Rev. 47 (1935) 947–957. doi:10.1103/PhysRev.47.947.

[46] S.F. Collins, G.W. Baxter, S.A. Wade, T. Sun, K.T. V. Grattan, Z.Y. Zhang, A.W. Palmer, Comparison of fluorescence-based temperature sensor schemes: Theoretical analysis and experimental validation, J. Appl. Phys. 84 (1998) 4649–4654. doi:10.1063/1.368705.

[47] C.D.S. Brites, A. Millán, L.D. Carlos, Lanthanides in Luminescent Thermometry, in: 2016: pp. 339–427. doi:10.1016/bs.hpcre.2016.03.005.

[48] G. Ghosh, Model for the thermo-optic coefficients of some standard optical glasses, J. Non. Cryst. Solids. 189 (1995) 191–196. doi:10.1016/0022-3093(95)00247-2.

[49] M. Reben, M. Środa, Influence of fluorine on thermal properties of lead oxyfluoride glass, J. Therm. Anal. Calorim. 113 (2013) 77–81. doi:10.1007/s10973-013-3047-x.

[50] T.P. Seward III, T. Vascott, High temperature glass melt property database for process modeling, Wiley-American Ceramic Society, 2005.

[51] C.G.B. Garrett, W. Kaiser, W.L. Bond, Stimulated Emission into Optical Whispering Modes of Spheres, Phys. Rev. 124 (1961) 1807–1809. doi:10.1103/PhysRev.124.1807.

[52] P. Haro-González, I.R. Martín, L.L. Martín, S.F. León-Luis, C. Pérez-Rodríguez, V. Lavín, Characterization of Er3+ and Nd3+ doped Strontium Barium Niobate glass ceramic as temperature sensors, Opt. Mater. (Amst). 33 (2011) 742–745. doi:10.1016/j.optmat.2010.11.026.

[53] C. Pérez-Rodríguez, L.L. Martín, S.F. León-Luis, I.R. Martín, K.K. Kumar, C.K. Jayasankar, Relevance of radiative transfer processes on Nd3+ doped phosphate glasses for temperature sensing by means of the fluorescence intensity ratio technique, Sensors Actuators B Chem. 195 (2014) 324–331. doi:10.1016/j.snb.2014.01.037.

[54] D. Ganta, E.B. Dale, J.P. Rezac, A.T. Rosenberger, Optical method for measuring thermal accommodation coefficients using a whispering-gallery microresonator, J. Chem. Phys. 135 (2011) 084313. doi:10.1063/1.3631342.